Ultrafast laser micro-stressing for correction of thin fused silica optics for the Lynx X-Ray Telescope Mission

Heng E. Zuo[a,c], Brandon D. Chalifoux[b,c], Ralf K. Heilmann[c], and Mark L. Schattenburg[c]

[a]MIT Dept. of Aeronautics & Astronautics, Cambridge, MA, USA 02139
[b]MIT Dept. of Mechanical Engineering, Cambridge, MA, USA 02139
[c]MIT Kavli Institute for Astrophysics and Space Research, Cambridge, MA, USA 02139

ABSTRACT

Fused silica exhibits high nonlinear optical response when exposed to ultrashort laser pulses, and the rapid development of femtosecond laser technology since the 1990s has greatly advanced the processing of such transparent materials. Since then, ultrafast laser micromachining has been widely implemented to remove materials or change material properties, from surface ablation to waveguide fabrication. Recently, we devised a potential use of this technique for optics precision correction of future space telescopes, for example the Lynx X-ray telescope mission. This novel mirror figure correction process provides a rapid and precise way of creating local micro deformation within the interior of thin mirrors, which then induces macro structural changes in surface figure to meet the stringent angular resolution requirements for the X-ray telescope. The method is highly controllable and deterministic, and the long-term stability of the laser-induced material changes makes it promising for future space telescope missions.

In this paper, we review the mechanisms and nonlinear optical phenomena of femtosecond laser interaction with fused silica. We also report on the current development of our laser pulses generation, focusing, imaging and an in-situ wavefront sensing systems, as well as our procedure for measuring and correcting mirror substrates. Preliminary experimental results of local deformation and stress changes in flat thin fused silica mirror substrates are shown, demonstrating the correctability of fused silica substrates within a capture range of 1 µm in surface peak-to-valley or 2″ in RMS slope using local laser micromachining. We also showed the laser induced integrated stress increases linearly with the micromachining density.

Keywords: ultrafast laser, figure correction, thin optics, fused silica, micro-stressing, X-ray telescope, Lynx

1. INTRODUCTION

1.1 Background on X-ray astronomy

X-ray astronomy observatories are designed to probe into an otherwise "invisible" universe by observing astrophysical phenomena across the X-ray spectrum, and to seek answers about the formation and evolution of galaxy clusters, supermassive black holes in active galactic nuclei, supernova remnants, binary stars, etc. Some existing X-ray observatories have enabled us to explore this high energy universe, such as NASA's Chandra X-ray Observatory and ESA's XMM-Newton. Chandra, launched in 1999, has successfully served the global astronomy community for the past 19 years with an unprecedented half-arcsecond angular resolution, despite its limited collecting area and narrow field of view.

Future X-ray space telescopes need to meet more stringent requirements for high resolution, large field of view and large effective area[1] in order to study astrophysical phenomena in fine detail. For instance, Lynx, a high-energy flagship mission concept funded for study by NASA for consideration in the 2020 Astrophysics Decadal Survey, intends to provide X-ray vision "with unique power to directly observe the dawn of supermassive black holes, reveal the drivers of galaxy formation, trace stellar activity including effects on planet habitability, and transform our knowledge of endpoints of stellar evolution."[2] The optics for Lynx are an assembly of densely-packed, thin, grazing-incidence mirrors with an outer diameter of 3 m and a total effective area greater than

Further author information: (Send correspondence to Heng E. Zuo)
E-mail: zuoh@mit.edu, Telephone: 1 617 803 9960

$2\,m^2$ at $1\,keV$. It will have an on-axis angular resolution of $0.5''$ half power diameter while maintaining the sub-arcsecond resolution out to $10'$ off-axis.

The special design of nested grazing-incidence optics, telescope mass constraints and economic considerations, make the manufacturing and correction of X-ray optics challenging. Current mirror fabrication methods include glass slumping,[3,4] silicon pore optics,[5] monocrystalline silicon polishing,[6] and mirror correction techneques including ion implanting,[7] piezoelectric film adjusting,[8] etc. are still quite limited in resolution and stability. The problem of correcting sub-arcsecond figure errors in thin mirrors with high precision and stability still remains to be developed with some new potential technologies.

1.2 Intro to ultrafast laser micromachining

Ultrafast or ultrashort pulsewidth lasers refer to lasers of extremely short pulse duration, typically on the order of femtosecond and picosecond range. The term "ultrafast laser micromachining" refers to technologies applying ultrafast lasers to remove materials or to change the properties of materials, for both absorptive and transparent substances.[9] Various topics related to this technique have been studied since the 90s, including the generation and development of femtosecond lasers,[10–12] nonlinear optical process,[13–15] laser-induced optical breakdown,[16–19] and micromachining applications.[20–22] These studies have helped the understanding of underlying mechanisms in ultrashort laser-matter interactions as well as advancing the technical development of practical applications of ultrafast lasers.

In general the absorption mechanisms of incident laser radiation vary for different materials, depending on laser intensity and pulsewidth. For opaque materials, linear processes dominate at long pulsewidths with low intensity, while nonlinear absorption of incident light becomes the main scheme at ultrashort pulsewidths and high intensity. For transparent materials, no terms corresponding to linear absorption from the incident light exist, so optical breakdown can only arise from nonlinear absorption of laser energy which excites electrons from the valence band to the conduction band. Damage in materials from ultrashort pulsewidth lasers is a combination of two nonlinear excitation mechanisms — photoionization and avalanche ionization — which contribute differently especially in the femtosecond domain.

1.2.1 Two nonlinear electron excitation mechanisms

Nonlinear photoionization and avalanche ionization both contribute to the nonlinear excitation of electrons, which leads to further plasma formation and optical breakdown, and they function under different conditions.

Photoionization is the physical process of direct excitation of electrons leading to ion formation, by interaction of photons from the incident laser field with an atom or molecule. The probability of photoionization depends on the energy of the photon and the target material, and an ionization threshold exists. At high laser intensities, several photons of energy below the ionization threshold may be simultaneously absorbed by an electron resulting in nonlinear multiphoton ionization. With even stronger laser intensity or longer wavelengths, the Coulomb well that binds a valence electron to its parent atom can be suppressed, such that the bounded electron may tunnel through a relatively low and narrow barrier, which is known as tunnelling ionization.[19]

Avalanche ionization refers to a series of photon-electron interaction processes, where a few initially free or previously nonlinearly excited electrons are further excited through phonon-mediated linear absorption, and acquire adequate kinetic energy to excite other bound electrons in the valance band.

1.2.2 Timescale of different physical phenomena during ultrafast laser-matter interaction

When enough bound electrons are excited and freed and their density reaches a threshold, an absorbing plasma is created with a natural frequency in resonance with the laser frequency, leading to an optical break-down of the transparent material. The absorption of the plasma is much greater than the absorption by initial extremely low density seed electrons, and the transparent material becomes opaque.

For long pulsewidths, the breakdown threshold field strength is lower and the laser-induced breakdown is dominated by avalanche ionization. The seed electrons are sparsely distributed inside the material, leading to large fluctuations and statistical behavior of optical breakdown.

For short pulsewidths, multiphoton ionization can directly generate free electrons, and the laser-induced breakdown threshold becomes more deterministic.[18] The laser energy absorption by the electrons is much faster in timescales compared to the energy transferring to the lattice. Therefore the electron-lattice scattering rates are not affected, and no thermal and mechanical stresses need to be considered because of minimized energy flow into the lattice,[17] resulting in reduced and minimized thermal damage as compared to longer pulsewidths, as well as improved precision of the induced material change in both shape and size. With tight focusing, the micromachined volumes inside the bulk of the material can be confined to the focal volume of the laser without causing absorption at the surface, in a volume as small as $0.008\,\mu m^3$.[23]

Figure 1 shows the timescale of relevant physical processes involved in the conversion from laser pulse energy to material changes. The absorption of photon energy occurs on tens of femtoseconds timescale. On a picosecond timescale, part of the optical energy absorbed by the electrons is transferred to the lattice. On the nanosecond timescale, a shock wave is emitted from the dense hot focal volume.[24,25] On the microsecond timescale, the thermal energy diffuses to the outside of the focal volume. With sufficiently high energy pulses, these processes leave permanent material structural changes through thermal or ionic motions.

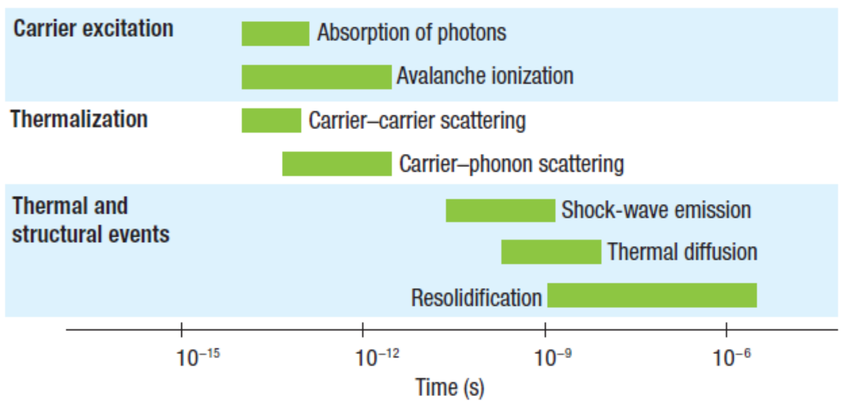

Figure 1: Timescale of the physical phenomena associated with the interaction of a femtosecond laser pulse with transparent materials. The green bars represent typical timescales for the relevant process, ranging from femtoseconds to microseconds.[9]

1.2.3 Advantages of ultrafast laser micro-processing

The nonlinear nature of ultrafast laser-matter interaction results in many unique advantages of such micromachining methods of transparent materials over other fabrication techniques, such as excimer lasers* Ultrafast laser micromachining has unique advantages especially in the visible and near infrared wavelength:

1. Heat diffusion outside the focal area is minimized and optical breakdown of materials is constrained to the focal volume, making the micromachining process precise and controllable.[26,27]
2. All seed electrons for the absorption can be generated through nonlinear ionization from the first tens of femtoseconds of a pulse, so the optical breakdown is a deterministic rather than a statistical process.[17]
3. The three-dimensional degree of freedom of the micromachining enables not only surface but also interior material processing, permitting fabrication of vertical structures.[28]
4. The material independence of absorption processes for some materials enable fabrication in compound substrates composing different materials.[9]

*Excimer lasers, using short ultraviolet wavelengths and popular for photochemical interaction with materials, is a technique that can achieve very fine feature sizes. Yet difficulties arise from in handling of corrosive gases and UV radiation damage of optics, making them undesirable for many industrial applications.

5. The ability of varying the focusing depth into the material can minimize the damage threshold and focusing aberrations.[19]
6. The long-term stability of the laser-induced index change is much better than traditional fabrication techniques,[9] and laser-induced stress change has been demonstrated.[29]

2. METHODS

Given the advantages of ultrafast laser micromachining, and the challenging requirements of high-resolution X-ray telescopes, we devised a process which applies this method to the correction of thin telescope mirrors. We call this method "micro-stressing" because it is the pulse induced stress in a sub-micron volume that we need to correct the mirror figure, unlike other applications of ultrafast laser micromachining. The details are described in this section.

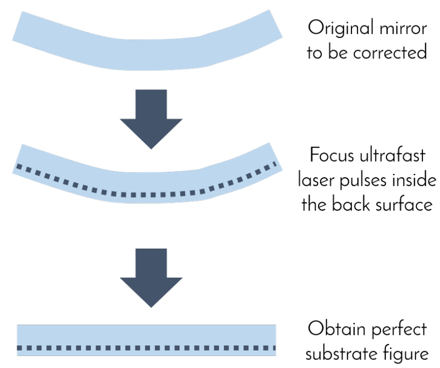

Figure 2: Demonstration of the process of ultrafast laser correcting thin optics on flat wafers. Pulses are focused inside the back surface of a mirror substrate, creating local stressed volumes inside the focal regions, causing substrate bending and inducing global substrate deformation. The method can be applied to curved mirrors with a different set-up to allow for 3D motion of the substrates.

Our initial experiments are performed on thin flat fused silica substrates to demonstrate the process, illustrated in Figure 2. Pulses are focused inside the back surface of a mirror substrate to be corrected, which has local shape errors due to fabrication or additional stresses caused by coatings, etc. Ultrashort laser pulses transfer energy to the excited electrons and alter the material inside the focal spot permanently. The substrate is then moved to expose a sequence of regions across the substrate, wherein the local machining density of these micro stressed regions is controlled in order to induce a 3D density map of induced stresses in the whole substrate. This process creates local stresses inside the laser focal regions causing substrate bending and stretching, and inducing global substrate deformation, therefore achieving our goal of substrate correction. The method could be adapted to curved mirrors, such as the hyperbolic and parabolic mirrors in Wolter Type I X-ray telescopes, though the set-up would be more complicated to involve at least 3D motion of substrates.

The advantages of this approach includes high precision and controllability, and great long-term stability. In addition, by changing the focusing depth inside the substrate we can control the bending moment exerted on the substrate and adjust its global curvature, in both concave and convex directions.

2.1 Experiment set-up

Our testing system mainly consists of four parts: a laser generating system, a laser focusing/imaging system, a substrate handling/positioning system and a wavefront sensing system. We used an existing chirped-pulse amplification laser system built in house at MIT to generate ultrashort pulses, which has a seed femtosecond laser oscillator followed by several amplifiers. The design is similar to a typical femtosecond chirped-pulse amplification laser system as described in many references.[14] After stretcher, amplifier and compressor stages, we obtain a infrared beam with wavelength $\lambda = 1047\,\text{nm}$, pulse duration of $\tau = 12\,\text{ps}$ and pulse frequency of $1\,\text{kHz}$.

The generated picosecond IR beam is then directed through an SHG (second harmonic generation) crystal to obtain a frequency doubled green beam of wavelength $524\,\text{nm}$. This conversion is mainly for ease of alignment and measurement. A low power CW green tracking laser is also added to the working beam to help with alignment.

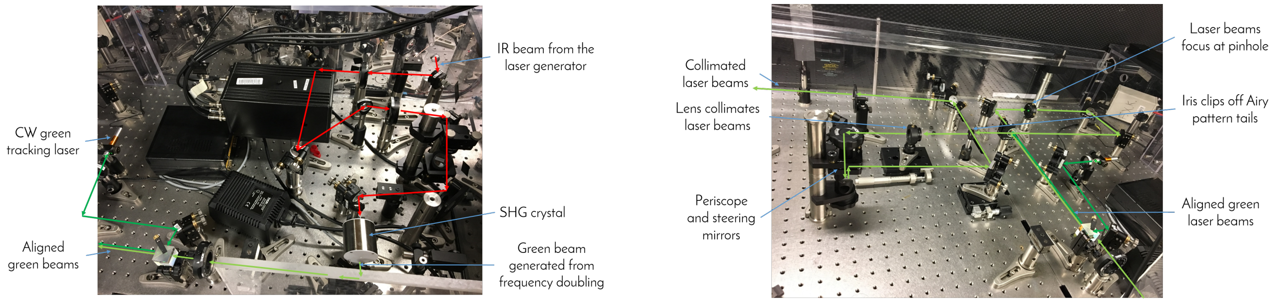

(a) IR beam passes through a SHG crystal to obtain a green beam, and another tracking beam is added to the working beam.

(b) The green beams are collimated and directed into a microscope.

Figure 3: Optical paths after the picosecond laser generator on the optical bench.

Then both beams are collimated and directed into a microscope and focused onto the substrate. The detailed optical paths are shown in Figure 3.

The laser focusing system is based on an inverted microscope, which directs and focuses the laser beam into a substrate from below, as shown in Figure 4. A high-speed translation stage (not shown in the picture) is mounted on top of the microscope objective lens, and the substrates are mounted onto the stage. A program built in C# is used to control the 2D translation of the stage, while the microscope sits on a stationary optical bench. A digital camera is mounted on the microscope to capture images.

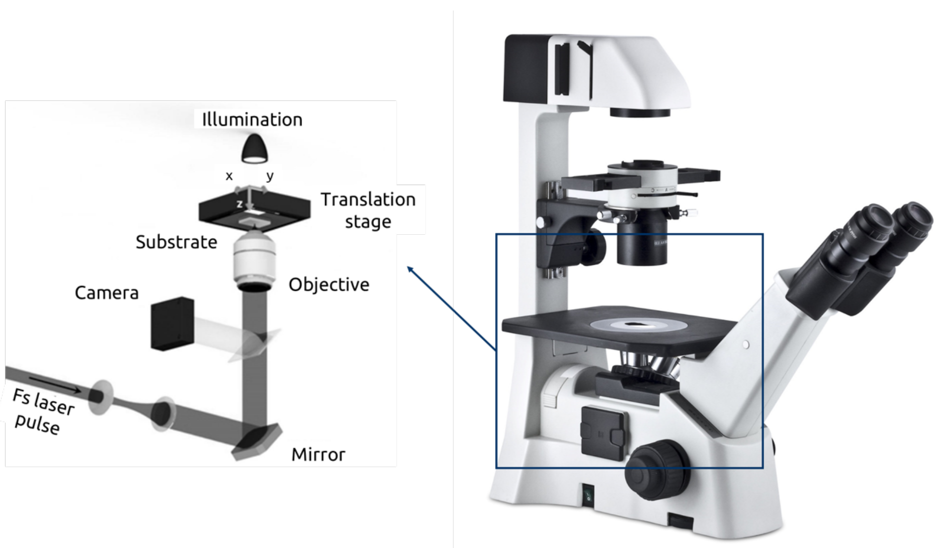

Figure 4: Laser beam focusing/imaging with the microscope.

Surface measurements are carried out by an in-situ Shack-Hartmann metrology tool,[7] which measures the surface slopes of a wavefront reflected from the substrate. A CCD camera captures these wavefront slope images, and surface height maps are reconstructed through some further analysis. This can be done either by fitting to a set of basis functions such as Zernike polynomials, or by direct integration of the surface slopes. Due to mechanical constraints, the in-situ Shack-Hartmann tool only measures the center 50 mm diameter areas of the substrates which are of 75 mm diameter.

2.2 Transmissivity measurement of fused silica

Many different ways have been proposed to measure the optical breakdown threshold, since this value varies dramatically for different systems. One practical way is to monitor changes in the refractive index as the fluence (energy per unit area) is increased, wherein the refractive index change in the laser-affected areas can be shown by changes of transmissivity and reflectivity.[30]

Our system outputs 12 ps FWHM pulses with energy up to 100 µJ/pulse at a center wavelength of 524 nm, with a repetition rate of 1 kHz. In order to measure single pulse transmissivity, the sample is moved laterally by 5 µm after each laser shot so that each measurement is at a fresh spot. The transmitted beam is then collected by a Thorlabs silicon detector mounted above the substrate. An appropriate neutral density filter is used before the detector. The signal from the detector is measured with a National Instruments DAQ device. We adjust the laser pulse energy with a half wave plate and polarizer combination, and measure the transmissivity of fused silica samples as shown in Figure 5.

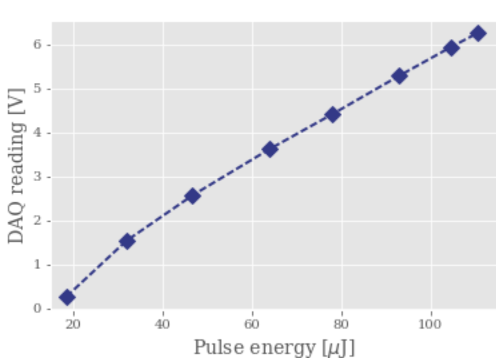

(a) Measurement of the laser pulse energy without any sample.

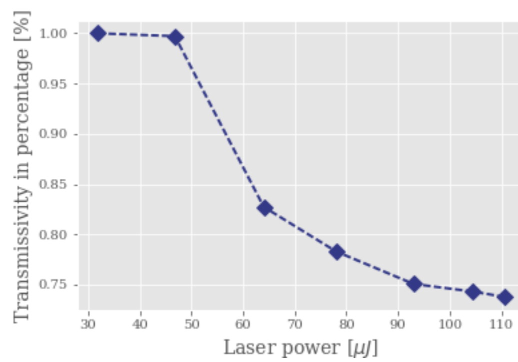

(b) Single pulse transmissivity measured at different pulse energies, and normalized with respect to the measurement on the left figure.

Figure 5: Single pulse transmissivity measurement of fused silica samples to infer the optical breakdown threshold of our system.

The left of Figure 5 shows the readings from NI DAQ device as a measurement of the laser pulse energy without substrates. These are used to calibrate measurements when there are samples present. The DAQ reading is almost linear with the pulse energy, as expected. The right figure shows single pulse transmissivity measured at different pulse energies, which are obtained by normalizing the DAQ readings with respect to the measurements in the left figure. The transmissivity decreases only above a certain pulse energy (about 50 µJ), and as the pulse energy increases the transmissivity decreases implying more intense optical breakdown. These measurements help us to choose the pulse energy to use in our experiments.

2.3 Process of micro-stressing fused silica substrates

We developed a procedure for micro-stressing and measuring the fused silica substrates, shown in Figure 6. This procedure requires only initial installation of the substrate onto the translation stage and no further manual handling to avoid placement-induced distortions.

In Step 2, the machining pattern refers to the distribution of laser shots, which is related to how we want to treat the substrate. Currently in order to study the effects of a small number of laser shots, a regular machining pattern in small regions is used, which is described in the next section. To correct a full mirror with varying shape errors in different places in the future, we will use this knowledge and apply a more complicated machining pattern with varying density, pulse energy, or even focusing depth.

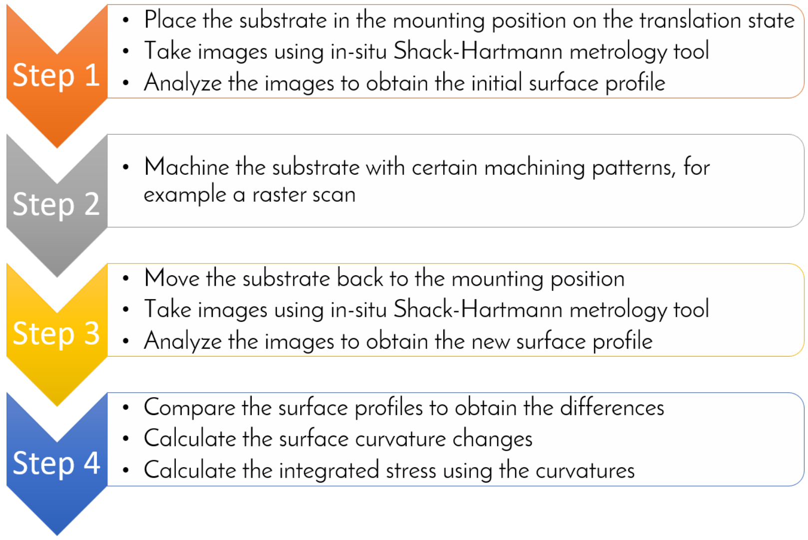

Figure 6: Procedure for fused silica substrates micro-stressing and measuring.

2.4 Machining patterns

In principle we would like to study how an individual laser shot creates the micro stress and bends the substrate, but this effect is very small and difficult to be directly detected. So, instead we "pave" a small region with many regularly spaced laser shots and try to observe the curvature change in that region of the substrate. The concept of this pattern is shown in Figure 7 and explained below.

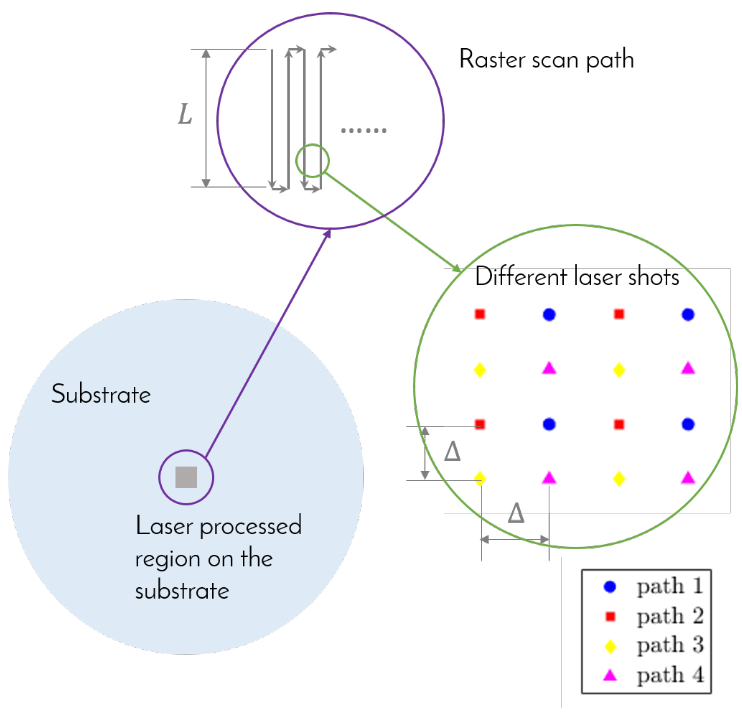

Figure 7: Illustration of the machining pattern used in this experiment.

The basic machining path is a raster scan, where the path has a rectangular shape. The substrate translates with the stage, which is controlled to move according to a raster scan path at a constant velocity in a horizontal plane. The vertical plane of laser beam focus is set to be the same for each experiment, by adjusting the knob on the microscope. During stage translation, the laser continues pulsing at its repetition frequency, so that each laser pulse produces a shot in a different spot on the substrate.

The parameters of interest here include:

- Machining interval 2Δ — distance between two successive laser shots on the substrate, which is set to be equal for both X and Y directions in this experiment;
- Machining length L — total length on each side of the laser processed area on the substrate;
- Machining density d — number of machined dots per square millimeter in the laser processed area.
- Machining depth t — focusing depth of laser shots below the substrate surface.

To study the influence of machining density, four separate raster scans are performed with an offset of Δ to each other in both directions. They are marked by different color dots in Figure 7, where each color dot indicates laser shots from the same raster scan. The distance between any two laser shots becomes Δ after processing completion, and the machining density increases linearly according to function $\frac{p}{4\Delta^2}$ where p is the number of the total scanning passes ranging from 0 to 4. The measurements are performed after each scan.

3. RESULTS

In this section we present results from a few fused silica samples after micro-stressing. The wafers are 75 mm in diameter, 500 µm thick and double-side polished. All of them used the same machining pattern as described earlier.

3.1 Fused silica substrate machining parameters and results

Table 1 summarizes the results of five fused silica samples tested during the past month. Note that the last five columns represent the final results, i.e. results after all four laser machining. The last four terms were calculated only in the laser treated areas on the substrates, with the calculation method explained in the next section. The machining depth were between 50 µm to 80 µm in these samples.

Sample label	Pulse energy [µJ]	Machining interval 2Δ [µm]	Machining length L [mm]	P-V change [µm]	RMS X slope change [$arcsec$]	RMS Y slope change [$arcsec$]	Principal integrated stress S_{xx} [N/m]	Principal integrated stress S_{yy} [N/m]
FS2018052501	50	10	5	0.6	1.8	1.6	75.0	117.2
FS2018053101	75	10	5	1.7	6.0	5.5	265.4	360.7
FS2018060102	50	10	5	0.5	1.2	1.7	32.7	39.3
FS2018060104	60	4	2	1.1	3.4	3.8	215.2	223.1
FS2018060203	80	4	2	1.8	4.7	6.1	291.2	326.8

Table 1: Fused silica substrates machining parameters and results

3.2 Example: sample FS2018060203

Here we show results from sample FS2018060203, which has gone through the highest machining density and highest pulse energy in the smallest machining area used for these experiments.

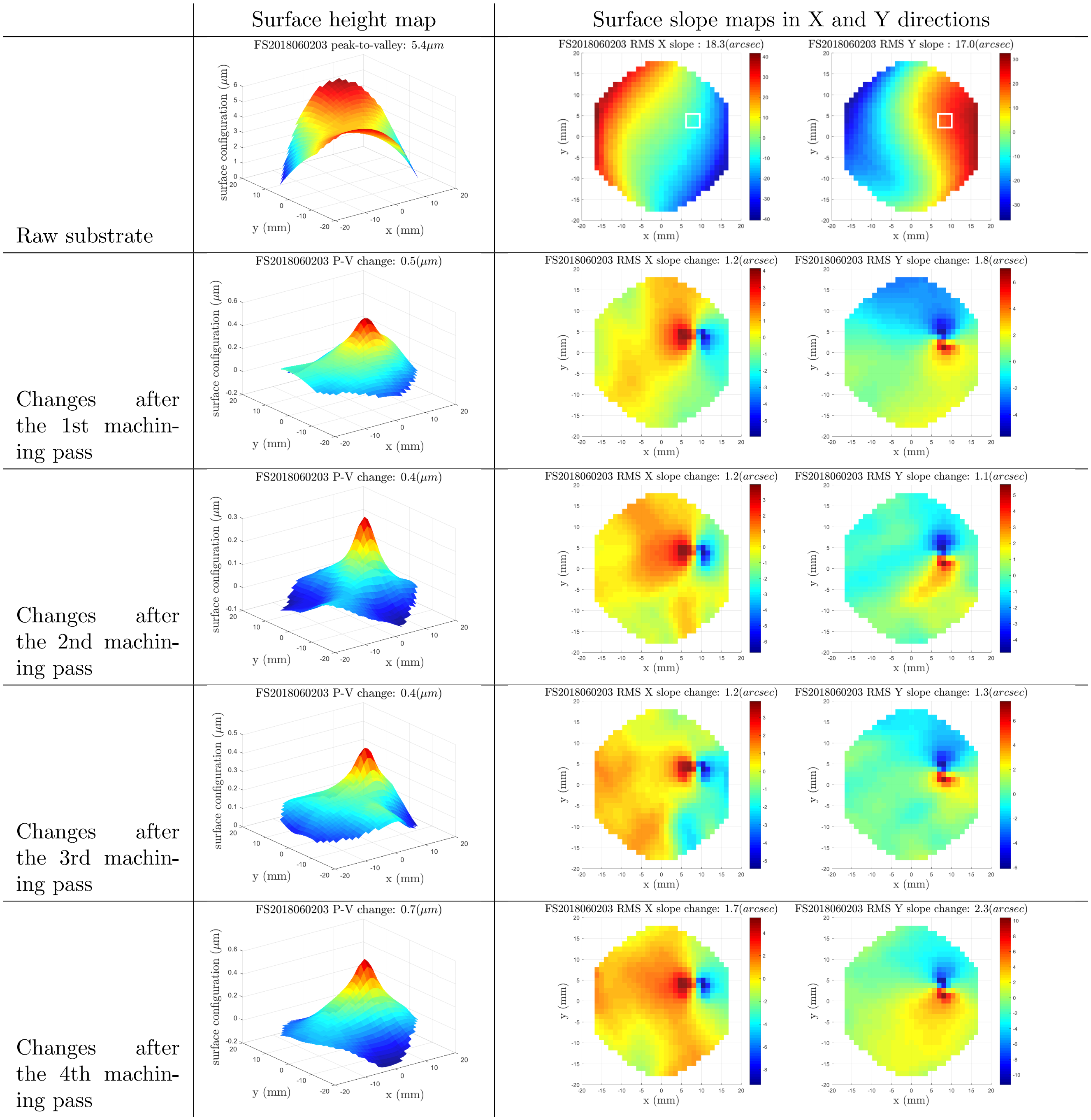

Figure 8: Measured changes in surface height and surface slopes after each machining pass. Machining was performed in the area indicated by the white boxes shown in the "Raw substrate" panel. Maps show differences in surface after the n^{th} machining pass compared to the $(n-1)^{th}$ pass.

3.2.1 Surface height and surface slopes

Figure 8 shows the continuous changes in both substrate surface height and surface slope maps in both X and Y directions as machining density increases. The first row is the raw substrate for comparison. The second row is obtained by subtracting initial Shack-Hartmann surface measurements from the measurements after the first machining pass. It shows the differences between two measurements caused by the ultrafast laser. It is clear that in all three figures the region experiencing drastic changes is in the area exposed to laser shots. Similarly, the second row shows the differences between the first and second laser machining passes, and so on. For each laser machining pass, we are able to change surface P-V by less than 1 µm, and surface slope by less than $2''$ in both X and Y directions, which shows the potential for mirror correction with high precision requirements.

3.2.2 Estimate of integrated stress in the laser machined area

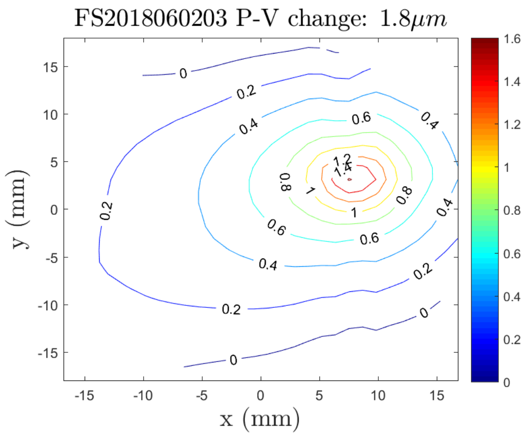

(a) Contour plot of the difference in surface profiles. Color bar unit is in µm

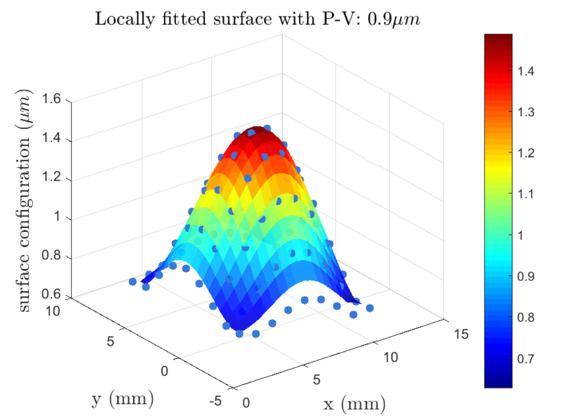

(b) Fitted local surface using polynomial functions. Color bar unit is in µm

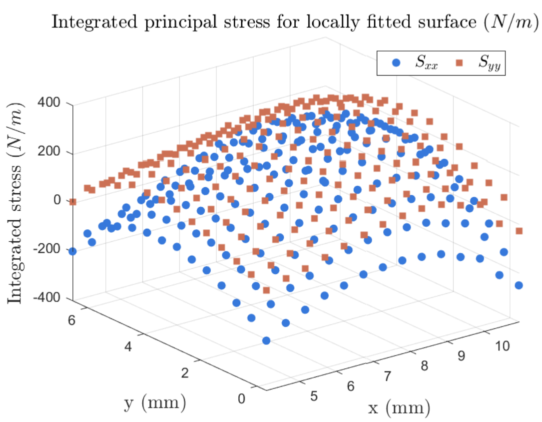

(c) Principal integrated stresses estimated from the fit.

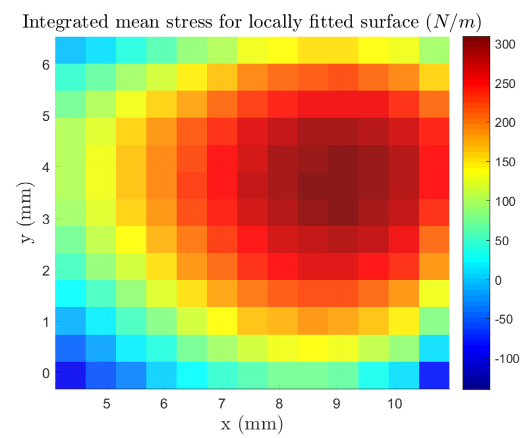

(d) Mean integrated stress (average of principal stresses) estimated from the fit.

Figure 9: Estimated integrated stress in the laser machined area.

We calculated the integrated stress in those areas in three steps:

1. Calculate the difference in surface profiles before and after the machining.
2. Select the machined area, and fit the local surface using fifth order polynomials.
3. Derive the local surface curvature from the fit and calculate the integrated stress using Stoney's equation:[31]

$$S_{xx} = \frac{E_s h_s^2}{6(1-\nu_s^2)}(\kappa_{xx} + \nu_s \kappa_{yy}) \tag{1}$$

$$S_{yy} = \frac{E_s h_s^2}{6(1-\nu_s^2)}(\nu_s \kappa_{xx} + \kappa_{yy}) \tag{2}$$

where E_s, ν_s are the Young's modulus and Poisson's ratio of the substrate, h_s is the substrate thickness, and κ_{xx}, κ_{yy} are the principal curvatures. In theory this formula only works for films on the surface of the substrate, yet since our laser focusing depth is small compared to the total thickness of the substrate this set of equations can give us good enough approximated answers.

The results are shown in Figure 9. (a) corresponds to step 1, and it shows the contour plot of the difference in surface profiles after all four machining passes. (b) corresponds to step 2, showing the local surface fitting with fifth order polynomials. (c) and (d) correspond to step 3, where the local surface curvatures in X and Y directions are derived, and plugged into the Stoney's equations to obtain integrated stresses. Note that the laser induced integrated stresses S_{xx} and S_{yy} in fused silica are tensile stresses, indicating that the micro-stresses regions experience increased density in agreement with previous results.[32] The measured deformation of a substrate by micro-stressing of a small region can be seen as a measurement of the process impulse response, which can be used to build a global correction algorithm, for example a linear function with variable weights for all impulse responses.[33]

We also calculated the integrated stresses as a function of the machining density, shown in Figure 10, and found that both S_{xx} and S_{yy} increase almost linearly with machining density, which also matches with the almost linear increase of RMS slope in both X and Y directions. The linear relationship indicates the possibility of correcting mirrors with arbitrary uniaxial shape errors by applying ultrafast laser pulses with appropriate machining density in different areas.

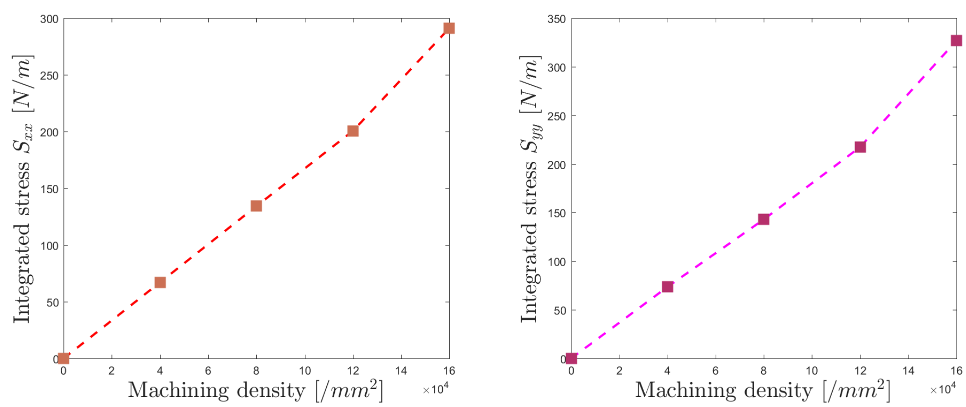

Figure 10: Measured integrated stress in fused silica substrates increases almost linearly with laser machining density.

4. CONCLUSION AND FUTURE WORK

In conclusion, we have demonstrated that ultrafast laser micro-stressing is a viable method of correcting mirror shape errors in thin fused silica optics. We have measured the global deformation of a full wafer from a local laser micro-stressing process, and have estimated the stress distribution in the laser treated areas. We found that large enough pulse energy and small enough machining interval are necessary to obtain observable substrate deformation. We also showed that fused silica substrates are correctable within 1 µm in surface P-V, and within $2''$ in RMS slopes with proper machining parameters. Finally, we demonstrated the potential for correcting optics by using the appropriate machining density in different areas of the mirror substrates.

We are still in an early stage in developing this method, and many additional demonstrations will be required. High strength and long-term stability are critical for space applications, so we need to conduct those tests. There are some other machining parameters that should be looked into, for example the focusing depth of laser shots. We will also build a finite element model of the microstressing process, which will provide us with more precise stress and strain results.

ACKNOWLEDGMENTS

This work has been supported by NASA APRA grants NNX14AE76G and NNX17AE47G. The authors give special thanks to Dr. Peter Krogen and Dr. Kyung-Han Hong at MIT RLE for helping with the picosecond laser system, to Dr. Lester Cohen for his kind advice, and to all members of MIT SNL for their support.

REFERENCES

[1] O'Dell, S. L., Allured, R., Ames, A. O., Biskach, M. P., Broadway, D. M., Bruni, R. J., Burrows, D. N., Cao, J., Chalifoux, B. D., Chan, K.-W., et al., "Toward large-area sub-arcsecond X-ray telescopes II," in [*Adaptive X-Ray Optics IV*], **9965**, 996507, International Society for Optics and Photonics (2016).

[2] Gaskin, J. A., Allured, R., Bandler, S. R., Basso, S., Bautz, M. W., Baysinger, M. F., Biskach, M. P., Boswell, T. M., Capizzo, P. D., Chan, K.-W., et al., "Lynx mission concept status," in [*UV, X-Ray, and Gamma-Ray Space Instrumentation for Astronomy XX*], **10397**, 103970S, International Society for Optics and Photonics (2017).

[3] Zhang, W. W., "Manufacture of mirror glass substrates for the NuSTAR mission," in [*SPIE Optical Engineering+ Applications*], 74370N, International Society for Optics and Photonics (2009).

[4] Zuo, H. E., Yao, Y., Chalifoux, B. D., DeTienne, M. D., Heilmann, R. K., and Schattenburg, M. L., "Recent progress on air-bearing slumping of segmented thin-shell mirrors for x-ray telescopes: experiments and numerical analysis," in [*Optics for EUV, X-Ray, and Gamma-Ray Astronomy VIII*], **10399**, 1039910, International Society for Optics and Photonics (2017).

[5] Collon, M. J., Vacanti, G., Günther, R., Yanson, A., Barriere, N., Landgraf, B., Vervest, M., Chatbi, A., van der Hoeven, R., Beijersbergen, M. W., et al., "Silicon pore optics for the ATHENA telescope," in [*Space Telescopes and Instrumentation 2016: Ultraviolet to Gamma Ray*], **9905**, 990528, International Society for Optics and Photonics (2016).

[6] Zhang, W. W., Allgood, K. D., Biskach, M. P., Chan, K.-W., Hlinka, M., Kearney, J. D., Mazzarella, J. R., McClelland, R. S., Numata, A., Olsen, L. G., et al., "Monocrystalline silicon and the meta-shell approach to building x-ray astronomical optics," in [*Optics for EUV, X-Ray, and Gamma-Ray Astronomy VIII*], **10399**, 103990S, International Society for Optics and Photonics (2017).

[7] Chalifoux, B., Burch, C., Heilmann, R. K., Yao, Y., Zuo, H. E., and Schattenburg, M. L., "Using ion implantation for figure correction in glass and silicon mirror substrates for x-ray telescopes," in [*Optics for EUV, X-Ray, and Gamma-Ray Astronomy VIII*], **10399**, 103991D, International Society for Optics and Photonics (2017).

[8] Walker, J., Liu, T., Tendulkar, M., Burrows, D., DeRoo, C., Allured, R., Hertz, E., Cotroneo, V., Reid, P., Schwartz, E., et al., "Design and fabrication of adjustable x-ray optics using piezoelectric thin films," in [*Optics for EUV, X-Ray, and Gamma-Ray Astronomy VIII*], **10399**, 103991K, International Society for Optics and Photonics (2017).

[9] Gattass, R. R. and Mazur, E., "Femtosecond laser micromachining in transparent materials," *Nature Photonics* **2**(4), 219–225 (2008).

[10] Backus, S., Durfee III, C. G., Murnane, M. M., and Kapteyn, H. C., "High power ultrafast lasers," *Review of Scientific Instruments* **69**(3), 1207–1223 (1998).

[11] Steinmeyer, G., Sutter, D., Gallmann, L., Matuschek, N., and Keller, U., "Frontiers in ultrashort pulse generation: pushing the limits in linear and nonlinear optics," *Science* **286**(5444), 1507–1512 (1999).

[12] Keller, U., "Recent developments in compact ultrafast lasers," *Nature* **424**(6950), 831–838 (2003).

[13] Brabec, T. and Krausz, F., "Intense few-cycle laser fields: Frontiers of nonlinear optics," *Reviews of Modern Physics* **72**(2), 545 (2000).

[14] Gibbon, P., [*Short pulse laser interactions with matter*], World Scientific Publishing Company (2004).

[15] Almeida, J. M., Almeida, G. F., Boni, L., and Mendonça, C. R., "Nonlinear optical properties and femtosecond laser micromachining of special glasses," *Journal of the Brazilian Chemical Society* **26**(12), 2418–2429 (2015).

[16] Von der Linde, D. and Schüler, H., "Breakdown threshold and plasma formation in femtosecond laser–solid interaction," *JOSA B* **13**(1), 216–222 (1996).

[17] Stuart, B. C., Feit, M. D., Herman, S., Rubenchik, A., Shore, B., and Perry, M., "Nanosecond-to-femtosecond laser-induced breakdown in dielectrics," *Physical Review B* **53**(4), 1749 (1996).

[18] Liu, X., Du, D., and Mourou, G., "Laser ablation and micromachining with ultrashort laser pulses," *IEEE Journal of Quantum Electronics* **33**(10), 1706–1716 (1997).

[19] Schaffer, C. B., Brodeur, A., and Mazur, E., "Laser-induced breakdown and damage in bulk transparent materials induced by tightly focused femtosecond laser pulses," *Measurement Science and Technology* **12**(11), 1784 (2001).

[20] Davis, K. M., Miura, K., Sugimoto, N., and Hirao, K., "Writing waveguides in glass with a femtosecond laser," *Optics Letters* **21**(21), 1729–1731 (1996).

[21] Dausinger, F., Lichtner, F., and Lubatschowski, H., [*Femtosecond technology for technical and medical applications*], vol. 96, Springer Science & Business Media (2004).

[22] Osellame, R., Cerullo, G., and Ramponi, R., [*Femtosecond laser micromachining: photonic and microfluidic devices in transparent materials*], vol. 123, Springer Science & Business Media (2012).

[23] Glezer, E., Milosavljevic, M., Huang, L., Finlay, R., Her, T.-H., Callan, J. P., and Mazur, E., "Three-dimensional optical storage inside transparent materials," *Optics Letters* **21**(24), 2023–2025 (1996).

[24] Schaffer, C. B., Nishimura, N., Glezer, E. N., Kim, A. M.-T., and Mazur, E., "Dynamics of femtosecond laser-induced breakdown in water from femtoseconds to microseconds," *Optics Express* **10**(3), 196–203 (2002).

[25] Sakakura, M., Terazima, M., Shimotsuma, Y., Miura, K., and Hirao, K., "Observation of pressure wave generated by focusing a femtosecond laser pulse inside a glass," *Optics Express* **15**(9), 5674–5686 (2007).

[26] Chichkov, B. N., Momma, C., Nolte, S., Von Alvensleben, F., and Tünnermann, A., "Femtosecond, picosecond and nanosecond laser ablation of solids," *Applied Physics A* **63**(2), 109–115 (1996).

[27] Sundaram, S. and Mazur, E., "Inducing and probing non-thermal transitions in semiconductors using femtosecond laser pulses," *Nature materials* **1**(4), 217 (2002).

[28] Nolte, S., Will, M., Burghoff, J., and Tuennermann, A., "Femtosecond waveguide writing: a new avenue to three-dimensional integrated optics," *Applied Physics A* **77**(1), 109–111 (2003).

[29] Dmitriev, V. and Stern, U., "Method and apparatus for locally deforming an optical element for photolithography," (Mar. 28 2017). US Patent 9,606,444.

[30] Wu, A. Q., Chowdhury, I. H., and Xu, X., "Femtosecond laser absorption in fused silica: Numerical and experimental investigation," *Physical Review B* **72**(8), 085128 (2005).

[31] Freund, L. B. and Suresh, S., [*Thin film materials: stress, defect formation and surface evolution*], Cambridge University Press (2004).

[32] Bellouard, Y., Champion, A., McMillen, B., Mukherjee, S., Thomson, R. R., Pépin, C., Gillet, P., and Cheng, Y., "Stress-state manipulation in fused silica via femtosecond laser irradiation," *Optica* **3**(12), 1285–1293 (2016).

[33] Allured, R., Ben-Ami, S., Cotroneo, V., Marquez, V., McMuldroch, S., Reid, P. B., Schwartz, D. A., Trolier-McKinstry, S., Vikhlinin, A. A., and Wallace, M. L., "Improved control and characterization of adjustable x-ray optics," in [*Optics for EUV, X-Ray, and Gamma-Ray Astronomy VII*], **9603**, 96031M, International Society for Optics and Photonics (2015).